Role of magnetism in the stability of the high-entropy alloy CoCrFeMnNi and its derivatives

Jakub Šebesta,[1,2] Karel Carva,[1] and Dominik Legut[2,3,*]

[1]*Charles University, Faculty of Mathematics and Physics, Department of Condensed Matter Physics, Ke Karlovu 5 121 16 Praha 2, Czech Republic*

[2]*Nanotechnology Centre, VŠB-TU Ostrava, 17.listopadu 2172/15, 708 00 Ostrava-Poruba, Czech Republic*

[3]*IT4Innovations, VŠB-TU Ostrava, 17.listopadu 2172/15, 708 00 Ostrava-Poruba, Czech Republic*

(Received 26 April 2019; revised manuscript received 1 October 2019; published 23 December 2019)

Multiprincipal element alloys, called high-entropy alloys represent a promising group of materials. They possess unique mechanical or electrical properties, which provide a wide range of potential applications. In general, mechanical or electrical properties of a material are influenced by the magnetic behavior. Therefore, in our work, we are exploring magnetic behavior of so-called "Cantor alloy" CoCrFeMnNi and its molybdenum based derivatives. Mo alloys were studied not only to carefully describe their properties but also to probe the magnetic behavior of the parent alloy by adding a nonmagnetic element. Based on *ab initio* calculations using the TB-LMTO-ASA (tight-binding linear-muffin-tin-orbital atomic-sphere approximation) method within CPA (coherent-potential approximation), we have found the ground-state magnetic structures of a particular alloy. We deal with various magnetic structures including complex structures beyond the simple FM or DLM phases. We show the influence of the presence of a particular element on the magnetic properties. It includes, e.g., magnitudes of magnetic moments or preferred magnetic phases. The calculations were extended by studying the magnetic exchange interaction employing the Liechtenstein formula. We clearly show the contribution of each element to the magnetism as a function of the composition or crystal structure. We provide a thorough description of magnetic behavior in the mentioned compounds.

DOI: 10.1103/PhysRevMaterials.3.124410

I. INTRODUCTION

High-entropy alloys (HEA) represent the so-called multiprincipal element alloys, based on several chemical elements unlike standard alloys. High number of constituents bring a variability of their properties, promising a wide range of applications. It includes great mechanical properties (e.g., high hardness [1] or extreme tensile strength [2]) as well as distinct electric properties (e.g., an anomalous Hall effect [3]).

In general, these alloys should be composed of at least five principal elements in a nearly equimolar ratio, where the concentration of principal elements stay in the range between 5%–35%. Consequently, high values of configuration entropy S_{conf} are reached. This constitutes HEAs due to stabilization of a solid solution phase. For a sufficiently high temperature, the entropic term ($-T\Delta S$, T is the temperature) can overcome the formation enthalpy H_{form} in the definition of Gibbs free energy G and favors the solid solution phase instead of an intermetallic phase [4–6].

The formation enthalpy H_{form} (1) is calculated there as a difference between the total energy of a relaxed alloy E^0_{alloy} and the weighted sum of total energies E^0_i of constituents present with concentrations c_i.:

$$H_{\text{form}} = E^0_{\text{alloy}} - \sum_i c_i E^0_i. \tag{1}$$

The most studied HEAs are alloys based on 3d elements [7]. Well known HEA belonging to this group is the "Cantor alloy" CoCrFeMnNi [8] with a fcc single solution phase. It is one of the primal and model HEAs. It exhibits exceptional ductility and toughness at low temperatures [9,10]. On the other hand, the alloy possesses only weak magnetism. It exhibits paramagnetic behavior at ambient temperatures [11]. Only at low temperatures experimental results suggest spin glass behavior below 25 K [12].

In recent reviews [1,13], the question of magnetic ordering in HEAs is recognized to be highly important. However, the number of experimental or theoretical studies is rather low. We recognize that magnetic order could largely affect mechanical properties and phase stability, as it is in the case of single constituent elements [14]. Hence it is appropriate to study magnetism in order to find the proper ground-state magnetic phase and to probe the role of each particular element. Furthermore, one of the most important parameters describing magnetic behavior is the critical temperature because it is related to the thermodynamic stability. Therefore studying magnetic exchange interactions is needed. They determine the value of the critical temperature as well as they provide knowledge of the interplay between particular constituents.

In the present work, we are focusing on the *ab initio* calculations of the Cantor alloys and its derivatives. We are interested in the ground-state magnetic structure and magnetic interactions in these compounds. We are looking beyond the simple structures as complex magnetic phases are included. The five studied derivatives contain Mo, which replaces in each case separately one of the five constituent elements of

*Corresponding author: dominik.legut@vsb.cz

the parent alloy. Mo has a rather similar electronic structure as the original elements, but its lack of magnetic moment allows us a deeper inside view into the role of magnetism here. Furthermore, the importance of an individual element for the stability and magnetic properties is studied as well. Such a thorough research has not been conducted so far.

II. METHODS

Calculations were performed using the tight-binding linear muffin-tin method based on the Green's function formalism within the atomic sphere approximation [15,16] (TB-LMTO-ASA). The local spin density approximation with Vosko-Wilk-Nursair exchange potential [17] and s, p, d atomic model were involved. The method offers calculation of a band structure in the scalar relativistic approximation, where the on-site spin-orbit coupling is added to the scalar relativistic hamiltonian, or in a fully relativistic way solving Dirac equation in the relativistic formalism [16]. To improve electrostatics in disordered systems, a basic screened impurity model was incorporated [18]. The TB-LMTO-ASA approach allows for straightforward implementation of the single-site coherent potential approximation (CPA) [19]. It was used for treating the chemical or magnetic disorder. The CPA is especially suitable for treating small perturbations as are small concentrations or similar atoms, which is the case of CoCrFeMnNi. It is a computationally efficient method, because instead of large supercells [20] only a small number of atomic sites is sufficient. For a simple ferromagnetic fcc cell only a single site is needed. More complicated magnetic ordering as antiferomagnetic or noncollinear one requires an increased number of sites.

In the construction of the elemental cell, various atomic radii were used based on their metallic radii [21]. Actually, the prescribed ratios between them had to be fulfilled as the cell volume changes. Then the lattice relaxation of parameters was done by changing the lattice parameter followed by an appropriate change of atomic radii, where energetic dependencies were evaluated. The employed calculation approach does not allow a distortion of the crystal structure. Therefore, in our calculation, a pristine crystal lattice is used. Muffin-tin based methods employing CPA without lattice relaxations (e.g., EMTO method) have already been applied in the field of HEAs in a number of cases [22,23]. Recently, an Al-based derivative of the Cantor alloy was successfully treated by the same method used by us (TB-LMTO-ASA) [24]. *Ab initio* calculations based on the supercell method have revealed only a small effect of lattice distortions regarding magnetic moments and equilibrium lattice constant in the Cantor alloy, while this effect was more significant in refractory HEAs [25]. These calculations also provide the lattice distortion energy, which is about 0.3 mRy [25] for the fcc phase of the Cantor alloy. This is a relatively small value when compared to energy differences that we encountered, and we do not expect it to vary significantly with magnetic order. Therefore it should not alter our main conclusions.

The calculation of the exchange interaction is possible employing the Liechtenstein formula. It is based on the obtained electron structure, where the LMTO potential parameters and averaged Green's function were employed [26,27].

TABLE I. Calculated lattice parameters and magnetic moments for selected elements. In brackets, experimental magnitudes of magnetic moments and lattice parameters are stated (Co [28,39,40], Cr [32,38,40], Fe [29,40,41], Mn [31,36], Ni [30,40,42], and Mo [40,43]).

	Lattice type	Magnetic phase	Magnetic moment (μ_B)		Lattice parameter (Å)
Co	hcp	FM	1.60	(1.58)	2.46 (2.51)
Cr	bcc	AFM	∼0	(0.4–0.6)	2.82 (2.88)
Fe	bcc	FM	2.15	(2.26)	2.80 (2.87)
Mn	bcc	AFM	0.87	(1.35–2.83)	8.42 (8.88)
Ni	fcc	FM	0.66	(0.61)	3.48 (3.52)
Mo	bcc	NM	–	(−)	3.18 (3.15)

The electron structure calculations were mainly performed in fully relativistic method. Due to the implementation of the Liechtenstein formula the results obtained in the scalar relativistic approximation were used as inputs for calculating pair exchange interaction J_{ij} in the effective Heisenberg's Hamiltonian [27]

$$H_{\text{eff}} = -\sum_{ij} J_{ij}\mathbf{e}_i \cdot \mathbf{e}_j, \tag{2}$$

where $\mathbf{e}_i$ represents unit vectors in the directions of magnetic spins. Observed differences between the scalar and fully relativistic approach will be discussed.

III. RESULTS AND DISCUSSION

A. Ground-state magnetic properties

Initially we studied ground-state magnetic and crystallographic phases. In order to evaluate the formation enthalpy H_{form} of CoCrFeMnNi and its derivatives, the energetic ground states of pure elements were found by lattice parameter optimizations. Elements with the following lattice types and magnetic structures were chosen. A nonmagnetic bcc molybdenum and ferromagnetic ordered hcp cobalt, bcc iron, and fcc nickel were calculated. The obtained lattice parameters almost correspond to the experimentally measured ones (Table I). Magnitudes of Co, Fe, and Ni moments fit well to the experimental values [28–30]. On the contrary, bcc Mn and bcc Cr possess significantly suppressed magnetic moments as compared to the experimental results [31,32] (Table I). Partly, it might be a consequence of the used method. It does not allow a lattice relaxation due to unavailable interatomic forces. Therefore, for a simplified magnetic structure, we did not obtain comparable values. Hence discrepancies could stem from the magnetovolume effect [16,33]. However, the key problem is the complicated magnetic structures of chromium and manganese, namely, spin density waves and the appearance of the noncollinear magnetism [32,34,35]. In the case of manganese, the antiferromagnetic (AFM) bcc structure with two atomic sites were selected as a initial magnetic structure. Probably due to the natural complex magnetic structure an underestimated lattice parameter was obtained in comparison to the experimental

value [36]. It also influences the magnitude of magnetic moments, because the calculated values dramatically vary with changing lattice size, which corresponds to discrepancies in their reported calculated values. They strongly depend on the used method and selected lattice form [31]. Also, experimental values are not uniform. For a simple AFM bcc model of Mn, the magnetic moment varies in the range of (1.35–2.83) μ_B [31]. Lattice parameters in Table I belong to the complex bcc structure with 58 atoms. The chromium possessing a complex magnetic structure did not converge to a magnetic state. It gives a roughly zero magnetic moments. For example, values between (0.4–0.8) μ_B can be found in the literature [32,37]. Nevertheless, the obtained lattice parameters fit quite well to the experimental one [38]. By comparison, it is only slightly underestimated.

For the Cantor alloy and its derivatives basic magnetic ordering phases (nonmagnetic NM, ferromagnetic FM, and antiferromagnetic AFM) were calculated. Also, more complicated structures were studied. The paramagnetic state with diluted magnetic moments (DLM) as well as a kind of noncollinear magnetic structures with a possible fluctuation of spin amplitude was simulated. We denote the latter as a spin density wave (SDW).

Due to the presence of the fcc lattice, we choose the structure, where magnetic spins rotated along the [111] direction, which is the direction of the stacking of the fcc lattice. For the comparison, also [100] and [110] directions were studied. The mentioned set of directions represents the main crystallographic directions in the cubic structure. In the case of the fcc alloy with significant magnetic moments (Table II) the lowest formation energy belongs to the SDW phase with [111] direction (Table III). Also, due to the close packed structure including small interatomic distances in the layer it possesses the highest magnitudes of magnetic moments (Table II). Besides, we study SDW phases in a similar way as in the bcc structure along [100] and [110] directions. Similarly, the [110] direction possessing smaller interatomic distances is almost more favorable. In Fig. 1, SDW phases related to the lowest formation enthalpy (Table III) are depicted. The Wigner-Seitz radii of the employed atoms were chosen as their metallic radii [44]. Use of differentiated atomic radii is important due to their effect on the total energy, lattice parameters, and magnetic moments. We checked that differences in atomic radii cannot be neglected.

1. CoCrFeMnNi: Cantor alloy

Initially we studied the parent Cantor alloy, primarily within the fcc structure, which is the experimentally reported one [8,45,46], and in *ab initio* calculations, it is considered as the high-temperature phase [47–49].

We found that for a simple fcc structure the Cantor alloy prefers paramagnetic state (Fig. 1) with tiny diluted magnetic moments (Table II). The obtained value of the equilibrium lattice parameter ($a = 3.48$ Å, respectively, $a = 3.49$ Å; depending on the observed magnetic order) is comparable to the experimental values ($a \sim 3.59$ Å) [8,50–52].

Noticeable magnetic moments were obtained only for more complicated noncollinear SDW structures described above. It indicates that the alloy likely prefers a noncollinear magnetic

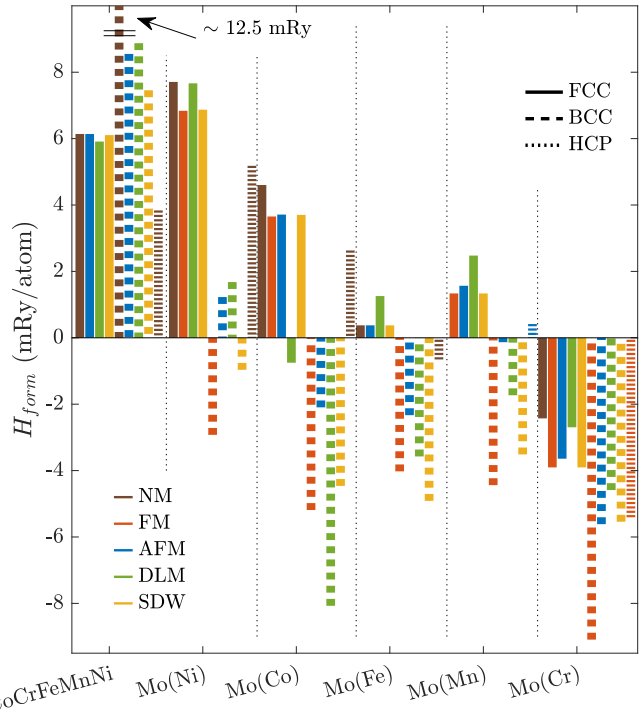

FIG. 1. Calculated formation enthalpies for studied CoCrFeMnNi and its derivatives dependent on the magnetic structure. In case of Mo derivatives, the substituted element is denoted.

structure. They also possess slightly higher values of the lattice parameter. Therefore, one should be aware that the lattice parameter likely increases with the proper magnetic structure, which seems to be complex here. The obtained values of the lattice parameter correspond to the range of calculated ones reported in the literature (e.g., $a = 3.50$ Å respectively, $a = 3.53$ Å for a (non)magnetic structure, VASP SQS method [53]). There, the values of lattice parameter appear in the range of ∼3.50 to ∼3.80 Å as calculated by various *ab initio* methods [47,53–56].

The CoCrFeMnNi alloy in the SDW phase shows ferrimagnetic ordering in each layer of the simulated system with magnetic moments of Co, Fe, and Ni atoms ordered in one direction, whilst moments of Cr and Mo preferred the opposite alignment. Generally, the ferrimagnetic phase is denoted here as FM since composing of a single magnetic sublattice with collinear moments. A ferrimagnetic ordering within a single layer is supported by the antiparallel behavior which was described in CoCrFeMnNi [45]. Moreover, the identical ferrimagnetic phase was reported in Ref. [47] (CPA) and our observations correspond to the distribution of magnetic moments in Ref. [57] (SQS). Likewise, it possesses similar directions and magnitudes of magnetic moments as in CoCrFeNi alloy [58]. Cr and Mn are elements with complicated antiferromagnetic magnetic structures. Hence the tendency to the ferrimagnetic structure instead of the ferromagnetic one is not surprising. Finally, the combination of FM elements with the AFM ones likely leads to a frustration of magnetic moments in collinear magnetic structures. Therefore the alloy should tend towards a complex magnetic structure. It is indicated by increasing magnitudes of magnetic moments and

TABLE II. Calculated lattice parameters and magnetic moments for CoCrFeMnNi and its derivatives depending on the lattice and the magnetic structure. Values of magnetic moments are sorted by a position of a particular element in the name of the appropriate alloy. In the case of SDW phase, magnetic moments rotate along the direction stated in the superscript. Magnitudes of magnetic moments on the single atomic site are shown. Fully relativistic calculations.

lattice		FCC							BCC							HCP		
Alloy	Magnetic structure	Lattice par. (Å)	Magnetic moments per atom (μ_B)					*Average*	Lattice par. (Å)	Magnetic moments per atom (μ_B)					*Average*	Lattice par. (Å)	Mag. mom. per atom (μ_B)	*Average*
CoCrFeMnNi	FM	3.48	~ 0						2.75	~ 0						2.46	~ 0	
	AFM	3.48	−0.01	0.00	0.20	−0.01	0.00	*0.04*	2.80	−1.31	0.66	2.07	1.73	−0.27	*0.57*			
	DLM	3.48	0.02	0.00	0.11	0.06	0.00	*0.04*	2.79	1.01	0.00	2.03	1.00	0.00	*0.81*			
	SDW$^{[111]}$	3.49	0.16	−0.11	0.82	−0.17	0.06	*0.15*										
	SDW$^{[100]}$	3.48	0.03	−0.02	0.50	−0.04	0.01	*0.10*	2.79	1.09	−0.08	2.09	1.33	0.14	*0.84*			
	SDW$^{[110]}$	3.48	0.00	−0.01	0.30	−0.03	0.00	*0.05*	2.79	1.27	−0.03	2.07	1.03	0.06	*0.96*			
MoCrFeMnNi	FM	3.62	−0.04	−0.12	1.09	−0.22	0.04	*0.15*	2.88	−0.12	−0.21	2.06	1.38	0.20	*0.66*	2.55	~ 0	
	AFM	3.62	0.00	0.02	1.01	0.14	0.00	*0.23*	2.87	−0.09	0.13	1.84	0.60	−0.07	*0.52*			
	DLM	3.62	0.00	0.00	0.98	0.17	0.00	*0.23*	2.88	0.00	0.00	2.00	1.09	0.00	*0.62*			
	SDW$^{[111]}$	3.61	−0.03	−0.11	0.99	−0.18	0.03	*0.14*										
	SDW$^{[100]}$	3.62	−0.01	−0.04	1.02	−0.16	0.00	*0.16*	2.88	−0.01	−0.03	2.01	1.06	0.02	*0.61*			
	SDW$^{[110]}$	3.62	−0.00	−0.02	0.97	−0.22	0.00	*0.15*	2.88	−0.05	−0.08	2.03	1.31	0.01	*0.66*			
CoMoFeMnNi	FM	3.58	0.48	−0.05	1.53	−0.78	0.10	*0.26*	2.87	1.44	−0.19	2.22	1.92	0.30	*1.14*	2.53	0.27 −0.05 0.78 −0.34 0.38	*0.37*
	AFM	3.59	−0.09	0.01	1.33	0.76	−0.01	*0.40*	2.89	−1.30	0.20	2.18	2.20	0.24	*0.61*			
	DLM	3.58	0.00	0.00	1.28	−0.65	0.00	*0.13*	2.87	0.91	0.00	2.12	1.87	0.00	*0.98*			
	SDW$^{[111]}$	3.59	0.48	−0.05	1.53	−0.78	0.10	*0.26*										
	SDW$^{[100]}$	3.59	0.13	−0.00	1.41	−0.76	0.02	*0.16*	2.87	−0.92	0.05	2.12	−1.85	−0.03	*−0.13*			
	SDW$^{[110]}$	3.59	0.05	−0.00	1.37	−0.90	0.00	*0.10*	2.88	1.21	−0.05	2.24	−0.61	0.04	*0.58*			
CoCrMoMnNi	FM	3.61	~ 0						2.87	−0.80	−0.20	−0.04	1.00	0.07	*0.01*	2.55	~ 0	
	AFM	3.61	0.00	0.00	0.00	0.04	0.00	*0.01*	2.86	0.88	0.21	0.06	0.94	−0.22	*0.37*			
	DLM	3.61	−0.01	0.00	0.00	0.12	0.00	*0.02*	2.87	0.92	0.00	0.00	1.44	0.00	*0.47*			
	SDW$^{[111]}$	3.59	~ 0															
	SDW$^{[100]}$								2.87	0.97	−0.02	−0.01	1.41	0.02	*0.47*			
	SDW$^{[110]}$								2.87	1.11	−0.03	−0.03	1.54	0.06	*0.52*			
CoCrFeMoNi	FM	3.61	0.48	−0.28	1.46	−0.08	0.11	*0.34*	2.87	1.28	0.06	2.14	−0.06	0.13	*0.71*			
	AFM	3.60	−0.03	0.01	1.20	0.00	0.00	*0.23*	2.85	0.63	0.03	1.84	0.06	−0.09	*0.49*	2.54	0.00 0.00 0.04 0.00 0.00	*0.01*
	DLM	3.60	0.00	0.00	1.21	0.00	0.00	*0.24*	2.87	0.87	0.00	2.04	0.00	0.00	*0.58*			
	SDW$^{[111]}$	3.61	0.48	−0.28	1.46	−0.08	0.11	*0.34*										
	SDW$^{[100]}$	3.60	0.10	−0.07	1.25	−0.02	0.02	*0.26*	2.87	0.95	−0.01	2.06	−0.01	0.03	*0.61*			
	SDW$^{[110]}$	3.60	0.00	−0.03	1.20	−0.00	0.00	*0.23*	2.87	1.20	0.06	2.10	−0.02	0.06	*0.67*			
CoCrFeMnMo	FM	3.60	0.10	−0.10	0.86	−0.14	−0.03	*0.14*	2.89	1.48	−0.03	2.18	1.71	−0.11	*1.05*	2.55	~ 0	
	AFM		not converged						2.87	−1.20	0.91	1.83	1.94	0.22	*0.74*			
	DLM	3.61	0.03	0.00	0.86	0.19	0.00	*0.22*	2.88	1.04	0.00	2.05	1.08	0.00	*0.83*			
	SDW$^{[111]}$		not converged															
	SDW$^{[100]}$	3.61	−0.01	−0.01	0.68	−0.09	−0.00	*0.11*	2.88	1.10	−0.02	2.07	1.06	−0.01	*0.84*			
	SDW$^{[110]}$	3.61	0.02	−0.03	0.76	−0.09	−0.01	*0.13*	2.89	1.32	−0.02	2.13	1.54	−0.04	*0.99*			
CoMoFeMoNi FM		3.70	0.64	−0.11	1.75	−0.11	0.12	*0.46*		–							–	

the decreasing formation enthalpy in the case of SDW phases (Tables II and III).

The calculated formation entropies H_{form} (Fig. 1) do not describe exactly the stability of studied alloys since other effects could be present there. One can mention the configuration entropy, the entropy of vibrations, etc. [47]. Besides, the absolute values of the formation enthalpy are influenced by the selected description of Cr, Mn atoms, because of their complicated magnetic structures. It leads to uncertainty in the position of the zero level of H_{form} in Fig. 1 for a particular alloy. Based on our calculations, we estimated the error in the range of (0.5–1.0) mRy/atom. Also, we study ground-state properties instead of the high temperature ones, generally reported in experiments. However, the results generally correspond to the reported ones obtained by different approaches [47,54,59].

Magnetic moment magnitudes in the fcc case are highly sensitive to the lattice volume [47]. We have found that the calculated magnitudes of magnetic moments of all elements (Table II) are rather suppressed as compared to their pure compounds. These are in good agreement with the previous calculation assuming the same volume that we considered [47]. The calculated energy differences between different magnetic phases for the fcc crystal structure are quite small. This conforms the unclear experimental reports on magnetism

TABLE III. Difference of the formation energy between three SDW phases and the FM phase ($\Delta H = H_{\text{form}}^{\text{SDW}} - H_{\text{form}}^{\text{FM}}$). The parent alloy is compared to NM and AFM phases.

Alloy	SDW phase [111]	[100]	[110]
		ΔH (μRy / atom)	
fcc			
Cantor (vs NM)	−34	−13	−3
Cantor (vs AFM)	−33	−12	−2
CoCrFeMnMo	–	49	33
MoCrFeMnNi	47	49	74
CoCrMoMnNi	−0.12	−0.12	−0.09
CoCrFeMoNi	0.05	174	228
CoMoFeMnNi	0.02	168	190
		ΔH (mRy / atom)	
bcc			
Cantor (vs NM)		−3.5	−5.0
Cantor (vs AFM)		0.4	−1.1
CoCrFeMnMo		3.7	2.0
MoCrFeMnNi		1.5	0.7
CoCrMoMnNi		−0.4	−0.9
CoCrFeMoNi		1.7	0.9
CoMoFeMnNi		3.6	4.0

below 25 K [12], and the presence of paramagnetic phase at ambient temperatures Refs. [11,60].

In addition, we have performed calculations of bcc and hcp crystal structures. They revealed that the hcp structure leads to the most stable ground state, which is in accordance with other studies [47,49]. Relatively small energy differences between crystal structures allow the occurrence of the high-temperature fcc phase according to the experiments.

2. *Mo derivatives*

To clarify the magnetic behavior in the Cantor alloy it is suitable to study derivatives of the parent CoCrFeMnNi besides. For this purpose, a nonmagnetic molybdenum substitution in fcc CoCrFeMnNi, where all atoms are in principal magnetic, was used. Mo derivatives were calculated in the fcc structure, which is suitable for a comparison with the parent Cantor alloy as well as in the bcc structure mostly reflecting their real structure [61] (the hcp structure was also checked to confirm the ground-state configuration). Optimized lattice parameters, obtained magnitudes of magnetic moments and the formation enthalpy are summarized in Table II and Fig. 1. Their behavior in bcc and fcc phases considerably differs.

For the bcc structure, simple ferrimagnetic structures prevail. They possess large magnetic moments on Co, Fe, and Mn atoms, whereas tiny moments appear on Ni and Cr atoms. The most significant on-site magnetic moments respect the ferromagnetic order. The opposite alignment occurs on Co and Ni atoms in particular. It depends on the studied magnetic phase and the alloy. One can notice that the most important elements for magnetic ordering seem to be Fe and Co. The absence of Fe atoms leads to the suppression of magnetic moments and to the SDW ground state. Similarly, in the FM phase, it changes directions of magnetic moments in comparison to the other derivatives. It shows that the directions

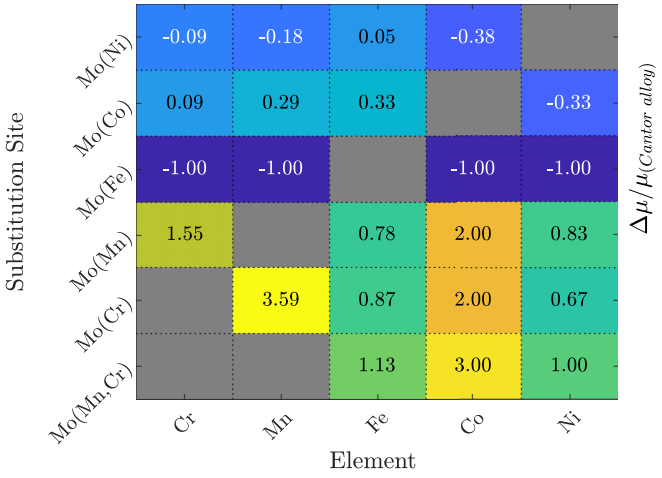

FIG. 2. Relative change of atomic magnetic moments in dependence on the position of Mo doping for alloys in the fcc structure. Magnitudes of magnetic moments of the parent alloy within the SDW magnetic structure were used for the comparison.

are driven by Fe magnetic moments. The substitution of Co leads to a paramagnetic DLM phase, which is favorable only in this case. It is accompanied by smaller Mn and Fe magnetic moments. An interplay between antiferromagnetic elements Cr and Mn was observed while they are substituted. The magnitudes of their magnetic moments become more positive when the counterpart element disappears (Table II). Calculating the formation enthalpy, we found that the most stable derivative from this point of view is the alloy with substituted Cr atoms. One can notice that it provides the highest values of magnetic moments, the induced Mo moment included. Slightly less favorable are the paramagnetic derivatives with substituted Co and the SDW one related to the Fe substitution.

In all the cases, the fcc structure leads to a strong suppression of magnetic moments, but partly the behavior remains unchanged. The order of the most stable Mo based derivatives and also the order of their ground-state magnetic phase is maintained. However, the energy differences especially between the magnetic phases are changed. Fe is still the most important element to establish the magnetic ordering. Moreover, it does not exist without the presence of Fe atoms. Taking into account the calculated formation enthalpies and obtained magnitudes of magnetic moments, a tendency towards relevant magnetic ordering appears either in the case of the substituted Cr or Mn, alternatively both of them. This indicates that the antiferomagnetic elements as Cr and Mn are probably obstacles for magnetic ordering, regardless of the crystallographic structure. This is likely pronounced in the increase in magnitudes of magnetic moments of FM phases obtained by the substitution of Cr or Mn in comparison to SDW phase of the parent alloy (Figs. 2 and 3). Any comparable rise of magnitudes of magnetic moment caused by the Mo substitution was not observed for bcc structures. One can also notice that chromium and manganese form a magnetic sublattice antiparallely ordered to the rest of elements similarly to the parent alloy, especially for FM phases. Besides they express their mutual competition in the magnitude of magnetic moments (Fig. 2). It might indicate the

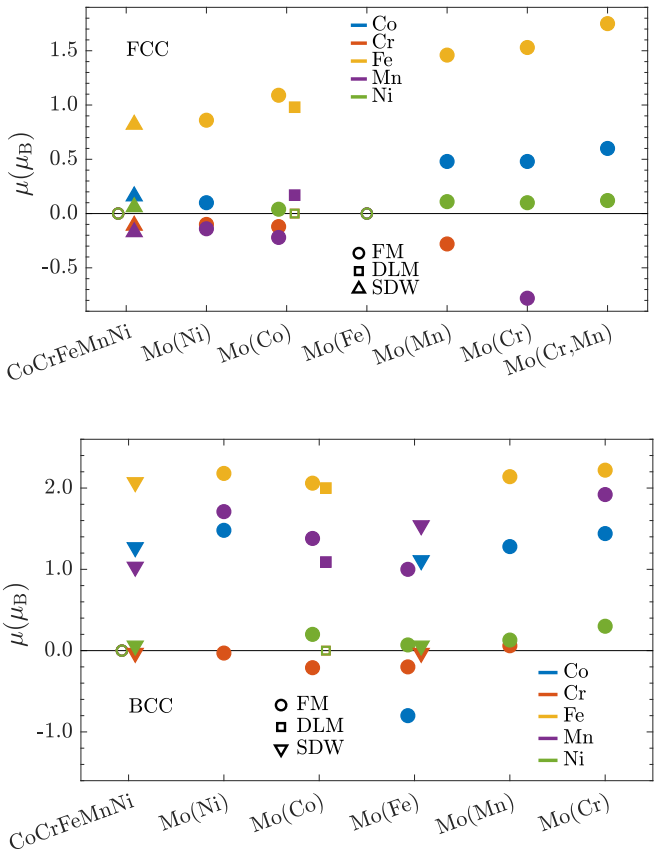

FIG. 3. Dependence of atomic magnetic moments on the crystal structure and the position of the Mo substitution. Alloys are sorted in order of the increasing total atomic number of the appropriate alloy. Unfilled point denotes almost zero magnetic moments.

existence of the spin frustration. The other substitutions with molybdenum, which reduce formation enthalpy H_{form}, tend to the paramagnetic DLM or the nonmagnetic state. The mentioned paramagnetic DLM state appears in the MoCrFeMnNi alloy for both structures. It may indicate the importance of Co for the magnetic ordering. Still it does not cause significant changes of magnetic moments in the fcc structure. Finally, it was observed that Ni has no significant effect on the evolution of magnetic moments. Its absence gives an FM state, but it leads to increase the formation enthalpy. At the end, we have to note that a substituted alloy might not form single-phase solution as it is reported [61].

B. DOS

To clarify the observed differences in values of magnetic moments obtained for different types of studied crystal structures, we calculated densities of states (DOS) for the parent alloys and its Mo derivatives (Fig. 4, see Ref. [62] for more details). The DOS obtained for the nonmagnetic structures allows us to deduct that the relatively high values of magnetic moments in the bcc crystal structure (Table II) are related to the presence of d states in the vicinity of the Fermi level [Figs. 4(a) and 4(c)]. Considering the Stoner model of itinerant magnetism, significant values of the DOS at the Fermi level are able to cause a band splitting leading to

TABLE IV. Calculated lattice parameters and magnetic moments for CoCrFeMnNi and its derivatives obtained within the scalar relativistic method.

Magnetic structure	Lattice	Lattice par. (Å)	Magnetic moments per atom (μ_B)				
			CoCrFeMnNi				
SDW	FCC	3.48	0.05	−0.05	0.34	−0.07	0.02
			MoCrFeMnNi				
DLM	BCC	2.88	0.00	0.00	1.96	1.07	0.00
	FCC	3.62	0.00	0.00	0.74	−0.03	0.00
			CoMoFeMnNi				
FM	BCC	2.87	1.40	−0.22	2.22	1.97	0.28
	FCC	3.59	0.35	−0.05	1.43	−0.77	0.08
			CoCrMoMnNi				
SDW	BCC	2.87	1.00	−0.04	−0.03	1.53	0.06
			CoCrFeMoNi				
FM	BCC	2.88	1.26	−0.04	2.14	−0.08	0.12
	FCC	3.61	0.36	−0.28	1.35	−0.08	0.08
			CoCrFeMnMo				
FM	BCC	2.88	1.38	−0.04	2.12	1.64	−0.11

the occurrence of itinerant magnetic moments. On the other hand, in the case of close packed fcc and hcp structures [Figs. 4(b) and 4(d)], d states are wider and stay further from the Fermi level. Therefore lower values of magnetic moments are assumed here, in general.

Finally, one can also compare the calculated DOS for the nonmagnetic bcc and fcc derivatives [Figs. 4(b) and 4(c)] with the appropriate magnitude of magnetic moments depicted in Fig. 3 for different Mo substitutions. There is a clear correspondence with the values of DOS at the Fermi lever for the bcc structures. However, the evaluation of the fcc case is more complicated due to the obvious small differences between DOS curves.

C. Exchange interaction

Having the relation between the composition and the magnetic structure or magnetic moments, we calculated the exchange interactions in the parent Cantor alloy and its derivatives for both bcc [Fig. 5(a)] and fcc [Fig. 5(b)] crystal structures. We expect to obtain an extra piece of information to the above-described behavior. In the calculations, the FM Green's functions were mostly used. The exceptions were the Cantor alloy, where significant nonzero moments were found only in the SDW case, and MoCrFeMnNi alloy, where interactions for parallel spins in the paramagnetic ground state were obtained. Further, fcc CoCrMoMnNi alloy was excluded due to the absence of magnetism, and the SDW phase was used for its bcc analog. Otherwise, the FM phase is the ground state (Fig. 1, Table II). We remind the readers that we are using the scalar relativistic approach instead of the fully relativistic one due to the implementation of the Liechtenstein formula [27]. In general, this approach leads to a small suppression of magnetic moments (Table IV). There are only two significant differences. The first one is the bcc CoCrMoMnNi alloy, where the directions and magnitudes of

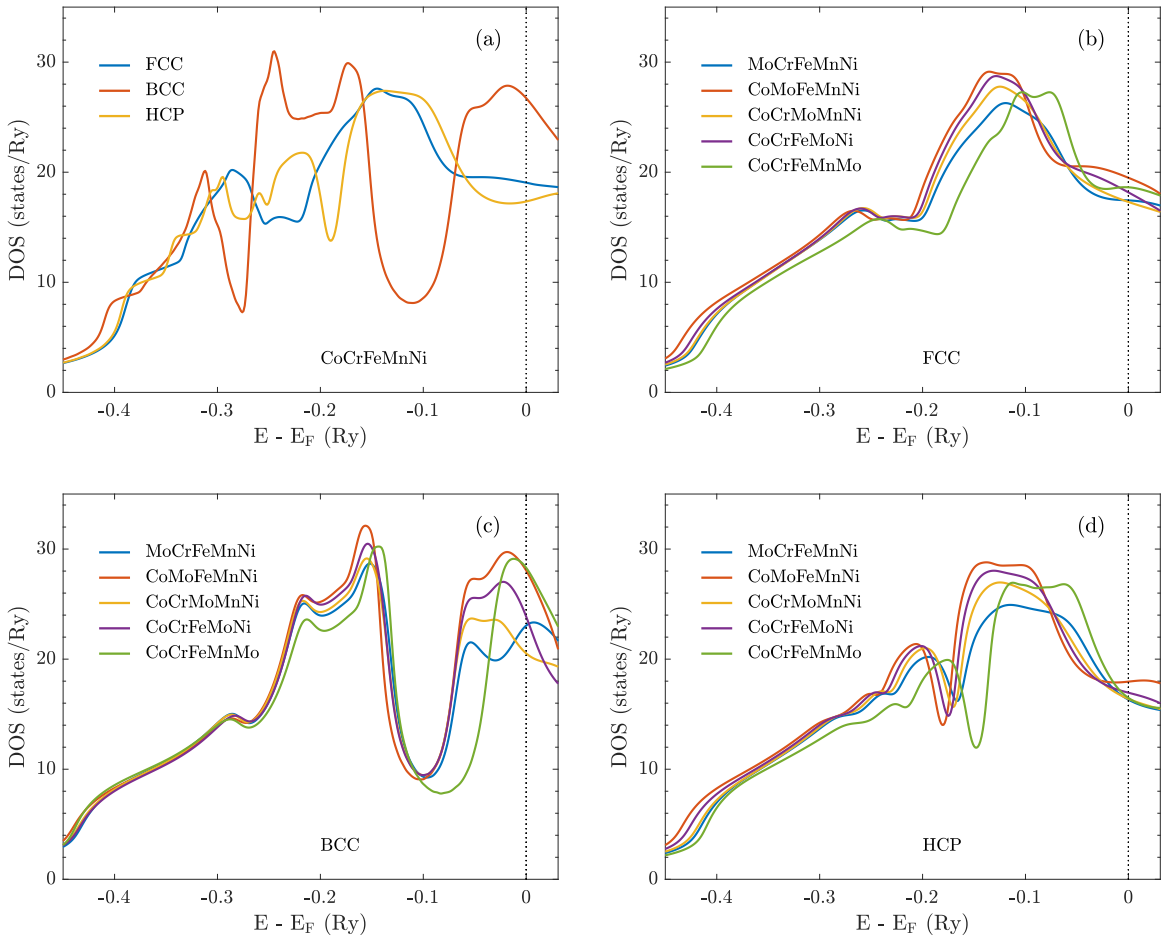

FIG. 4. Calculated DOSes for the nonmagnetic parent CoCrFeMnNi alloy and Mo derivatives. Energy zero marks the Fermi level. The spin polarized results are shown and more details are given in Ref. [62].

magnetic moments are changed. The second one is the fcc CoCrFeMnMo, which appears to be nonmagnetic in the scalar relativistic approach.

Our analysis shows, that the dominant interactions in fcc and bcc structures differ by one order of magnitude (Fig. 5). It confirms larger magnetic moments and the tendency to the FM ordering for the bcc structure (Fig. 1). We can assume that the difference is caused by the crystal symmetry and not by the volume effect, because the equilibrium lattice parameters refer to the same Wigner-Seitz radii for both bcc and fcc structures. Exchange interactions in the bcc structure [Fig. 5(a)] are dominated by ferromagnetic interactions of Co,

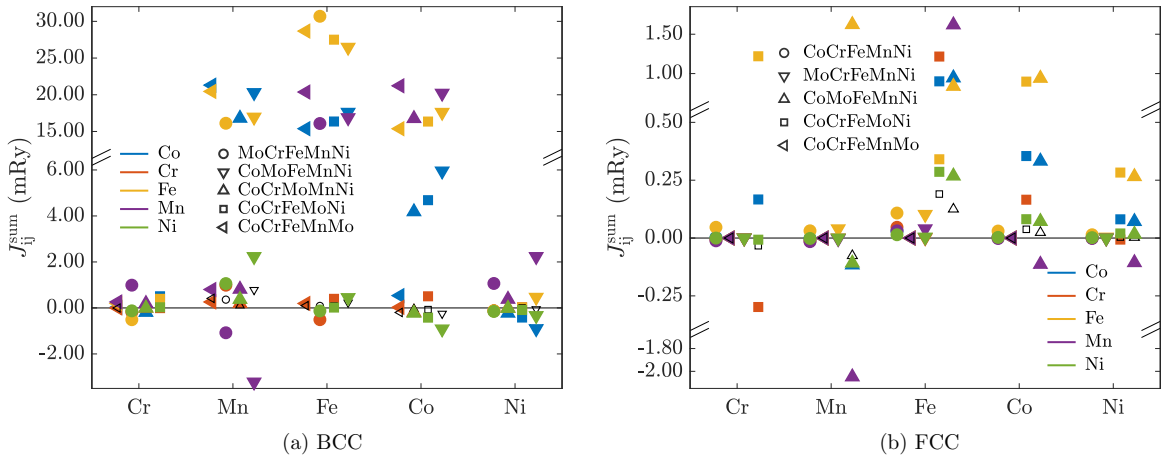

FIG. 5. Sums of exchange interaction J_{ij} in bcc and fcc crystal structures with resolved alloys and counterparts. The sum is over ten nearest neighbor shells. Unfilled point denotes interactions related to Mo atoms.

Fe, and Mn atoms, which likewise show the largest magnetic moments. The interactions related to Cr and Ni atoms are even weaker. It corresponds to their small magnetic moments in their various alignments. It comes from the interplay of their comparable parallel and antiparallel exchange interactions. The DLM phase in the case of MoCoFeMnNi should prevail due to the loss of strong ferromagnetic interactions originating from the Co atoms, since the magnetic ordering relies only on diluted Fe atoms.

The situation in the fcc structure [Fig. 5(b), Table II] is much more complicated due to the nonexistence of such dominant interactions as in the case of the bcc structure (similar to [23]). The most significant interactions are related only to Fe atoms. Depending on the position of the Mo substitution, the interactions with Co, Cr, and Mn become important. In comparison to the bcc structure, where Cr related interactions are negligible, similar interactions are essential in the case of fcc CoCrFeMoNi alloy thanks to the relatively weak exchange interactions and the absence of the Mn counterpart.

The fact that the most important exchange interactions rely on Fe atoms confirms their importance for magnetic ordering (Table II). Similarly, Co related interactions are also significant. Their absence within the structure leads to the DLM state (Fig. 1). It is observed that interactions related to Cr and Mn atoms are strengthened if the counterpart element is absent. It likely proves their mutual dislike in the system as was already discussed above (Fig. 2). We suppose that the observed dependence of magnitudes of Fe magnetic moments on the composition (Fig. 3) likely comes from mutual interactions with other atoms as we observed in Fig. 5(b), especially with the antiparallel elements. A similar feature does not occur in the case of the bcc structure (Fig. 3) probably due to the presence of strong ferromagnetic exchange interactions related to Fe atoms [Fig. 5(a)].

We would like to point out that despite using the scalar relativistic approach in our calculation of pair exchange interactions, which cause a little mismatch with full-relativistic results (Tables II and IV), the significance of Fe and Co atoms for magnetic ordering is confirmed by its very strong exchange interactions. Similarly, the correlation between the enhanced exchange interactions and strong magnetic moments in the case of bcc structures was shown.

D. Layered CoCrFeMnNi

In addition to the investigation of nonmagnetic substitution (e.g., molybdenum), we study the importance of a particular element in the CoCrFeMnNi alloy by a layer system with the varying concentration of elements, where the total concentration was kept constant. This allows us to compare the total energy due to the same total composition. We employ the SDW phase along the [111] direction possessing the highest magnetic moments.

A periodic system composed of four different layers was chosen. In the first layer atomic concentrations were lowered by 8% and 14% per site for a selected element.

We have obtained the dependence of the total energy and the magnetic moment caused by the suppression of the selected element, see (Fig. 6). Due to the small number of layers in the simulation, the effect of the underdoped first layer does not prevail. The resulting complex behavior leads to energy curves, which differs from our previous result. Therefore calculating much larger and more time-consuming layered structures is needed. It might be the scope of a future study. However, we observed a similar behavior as for the nonmagnetic substitutions in the dependence of magnetic moments magnitudes in the first layer on the suppressed element (Fig. 6) which is similar to the dependence on the Mo substitution (Fig. 3).

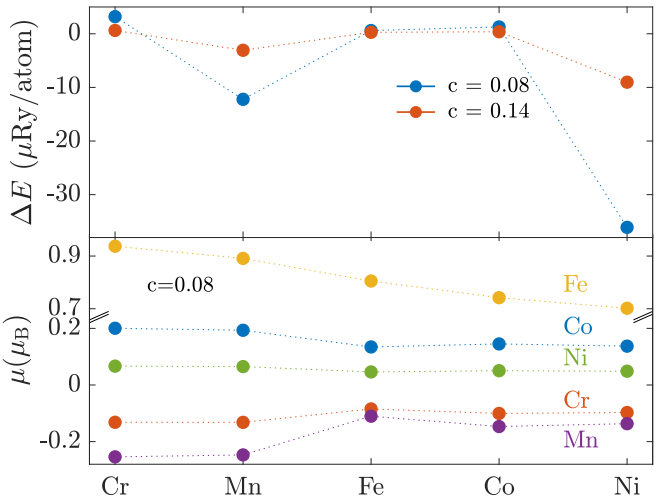

FIG. 6. Dependence of the total energy difference and magnitudes of magnetic moments on the selective underdoping of a particular element in the reference layer. The total stoichiometry is preserved and x axis denotes the suppressed element with a given concentration c in the reference layer. The change of the total energy is related to the energy of the unperturbed alloy ($\Delta E = E_{\text{tot}} - E_{\text{tot}}^{\text{Cantor}}$). Magnetic moments are related to the reference layer, where elements are distinguished by colors.

The obtained similarity between the Mo substitutions and varied concentrations proves the use of nonmagnetic substitution serves as a good probe to the magnetic behavior in such alloys. Furthermore, it also confirms that Cr and Mn atoms significantly suppress magnetism in such alloy.

IV. CONCLUSIONS

By using the Mo substitutions in CoCrFeMnNi alloy, we investigate the contribution of a particular constituent element to the alloy stability. We treated a wide range of magnetic structures. It includes complex SDW structures beyond common FM or DLM structures. Likewise, thanks to the nonmagnetic substitution we evaluated the contribution of a particular element to magnetic behavior as well as the preferred magnetic ground state.

Generally, we found the suppression of magnetism for the investigated fcc and hcp crystal structures with respect to the bcc one. It is the bcc structure that carries well pronounced magnetic behavior with high values of magnetic moments.

Calculations showed that the parent Cantor alloy in the high temperature fcc phase tends to the paramagnetic DLM state, but a complicated noncollinear magnetic ordering can not be excluded as well due to the observed

small energy differences. Here, tiny magnetic moments are expected.

Based on studying Mo substitutions, the crucial role of Fe and Co atoms to establish magnetic ordering was discovered. For fcc structures we found that nonzero magnetic moments rely on the presence of Fe atoms. In the bcc structure, their absence leads to the FM ground state with suppressed magnetic moments of the rest atoms, whereas the absence of Co atoms leads to the DLM phase for both crystal structures.

Furthermore, calculations reveal a destabilization effect of Mn and Cr atoms. Not only does its absence decrease the formation enthalpy as showed in the case of Mo-derivatives or layered CoCrFeMnNi systems but it also shifts the system towards the magnetic state. Therefore we assume that Mn and Cr atoms likely act as obstacles for the magnetic state. We can sum up that except for the case of substituted Co and Fe atoms the Mo derivatives tend to acquire FM ordering in both fcc and bcc lattice.

ACKNOWLEDGMENTS

This work was supported by the European Regional Development Fund in the IT4Innovations national supercomputing center - path to exascale project, Project No. CZ.02.1.01/0.0/0.0/16_013/0001791 within the Operational Programme Research, Development and Education and Grant No. 17-23964S of the Czech Science Foundation and CZ-AT Mobility Project No. 8J18AT004.

[1] O. N. Senkov and C. F. Woodward, Microstructure and properties of a refractory $NbCrMo_{0.5}Ta_{0.5}TiZr$ alloy, Mater. Sci. Eng.: A **529**, 311 (2011).

[2] A. Kuznetsov, D. Shaysultanov, N. Stepanov, G. Salishchev, and O. Senkov, Tensile properties of an AlCrCuNiFeCo high-entropy alloy in as-cast and wrought conditions, Mater. Sci. Eng.: A **533**, 107 (2012).

[3] Y.-F. Kao, S.-K. Chen, T.-J. Chen, P.-C. Chu, J.-W. Yeh, and S.-J. Lin, Electrical, magnetic, and Hall properties of $Al_xCoCrFeNi$ high-entropy alloys, J. Alloys Compd. **509**, 1607 (2011).

[4] E. J. Pickering and N. G. Jones, High-entropy alloys: A critical assessment of their founding principles and future prospects, Int. Mater. Rev. **61**, 183 (2016).

[5] M.-H. Tsai and J.-W. Yeh, High-entropy alloys: A critical review, Mater. Res. Lett. **2**, 107 (2014).

[6] M. F. del Grosso, G. Bozzolo, and H. O. Mosca, Determination of the transition to the high entropy regime for alloys of refractory elements, J. Alloys Compd. **534**, 25 (2012).

[7] D. Miracle and O. Senkov, A critical review of high entropy alloys and related concepts, Acta Material. **122**, 448 (2017).

[8] B. Cantor, I. Chang, P. Knight, and A. Vincent, Microstructural development in equiatomic multicomponent alloys, Mater. Sci. Eng.: A **375-377**, 213 (2004).

[9] F. Otto, A. Dlouhý, C. Somsen, H. Bei, G. Eggeler, and E. George, The influences of temperature and microstructure on the tensile properties of a CoCrFeMnNi high-entropy alloy, Acta Materialia **61**, 5743 (2013).

[10] A. Gali and E. George, Tensile properties of high- and medium-entropy alloys, Intermetallics **39**, 74 (2013).

[11] P. Yu, L. Zhang, H. Cheng, H. Zhang, M. Ma, Y. Li, G. Li, P. Liaw, and R. Liu, The high-entropy alloys with high hardness and soft magnetic property prepared by mechanical alloying and high-pressure sintering, Intermetallics **70**, 82 (2016).

[12] K. Jin, B. C. Sales, G. M. Stocks, G. D. Samolyuk, M. Daene, W. J. Weber, Y. Zhang, and H. Bei, Tailoring the physical properties of Ni-based single-phase equiatomic alloys by modifying the chemical complexity, Sci. Rep. **6**, 20159 (2016).

[13] Y. Ikeda, B. Grabowski, and F. Körmann, Ab initio phase stabilities and mechanical properties of multicomponent alloys: A comprehensive review for high entropy alloys and compositionally complex alloys, Mater. Charact. **147**, 464 (2019).

[14] G. Hausch, Elastic constants of Fe-Pt alloys. I. Single crystalline elastic constants of $Fe_{72}Pt_{28}$, J. Phys. Soc. Jpn. **37**, 819 (1974).

[15] H. L. Skriver, *The LMTO Method: Muffin-Tin Orbitals and Electronic Structure* (Springer, Berlin, 2012).

[16] I. Turek, V. Drchal, J. Kudrnovsky, M. Sob, and P. Weinberger, *Electronic Structure of Disordered Alloys, Surfaces and Interfaces* (Kluwer, Boston, 1997).

[17] S. H. Vosko, L. Wilk, and M. Nusair, Accurate spin-dependent electron liquid correlation energies for local spin density calculations: A critical analysis, Can. J. Phys. **58**, 1200 (1980).

[18] P. A. Korzhavyi, A. V. Ruban, I. A. Abrikosov, and H. L. Skriver, Madelung energy for random metallic alloys in the coherent potential approximation, Phys. Rev. B **51**, 5773 (1995).

[19] B. Velický, S. Kirkpatrick, and H. Ehrenreich, Single-site approximations in the electronic theory of simple binary alloys, Phys. Rev. **175**, 747 (1968).

[20] D. Holec, D. Legut, L. Isaeva, P. Souvatzis, H. Clemens, and S. Mayer, Interplay between effect of Mo and chemical disorder on the stability of β/β_0−TiAl phase, Intermetallics **61**, 85 (2015).

[21] N. N. Greenwood and A. Earnshaw, *Chemistry of the Elements*, 2nd ed. (Butterworth-Heinemann, Oxford, 1997).

[22] F. Tian, L. K. Varga, N. Chen, L. Delczeg, and L. Vitos, Ab initio investigation of high-entropy alloys of 3*d* elements, Phys. Rev. B **87**, 075144 (2013).

[23] S. Huang, E. Holmström, O. Eriksson, and L. Vitos, Mapping the magnetic transition temperatures for medium- and high-entropy alloys, Intermetallics **95**, 80 (2018).

[24] J. Kudrnovský, V. Drchal, F. Máca, I. Turek, and S. Khmelevskyi, Electron transport in high-entropy alloys: $Al_xCrFeCoNi$ as a case study, Phys. Rev. B **100**, 014441 (2019).

[25] H. Song, F. Tian, Q.-M. Hu, L. Vitos, Y. Wang, J. Shen, and N. Chen, Local lattice distortion in high-entropy alloys, Phys. Rev. Mater. **1**, 023404 (2017).

[26] A. Liechtenstein, M. Katsnelson, V. Antropov, and V. Gubanov, Local spin density functional approach to the theory of exchange interactions in ferromagnetic metals and alloys, J. Magn. Magn. Mater. **67**, 65 (1987).

[27] I. Turek, J. Kudrnovský, V. Drchal, and P. Bruno, Exchange interactions, spin waves, and transition temperatures in itinerant magnets, Phil. Mag. **86**, 1713 (2006).

[28] P. Marcus and V. Moruzzi, Equilibrium properties of the cubic phases of cobalt, Solid State Commun. **55**, 971 (1985).

[29] J. I. Beltrán, L. Balcells, and C. Martínez-Boubeta, Interfacial geometry dependence of the iron magnetic moment: The case of MgO/Fe/MgO, Phys. Rev. B **85**, 064417 (2012).

[30] S. E. Apsel, J. W. Emmert, J. Deng, and L. A. Bloomfield, Surface-Enhanced Magnetism in Nickel Clusters, Phys. Rev. Lett. **76**, 1441 (1996).

[31] D. Hobbs, J. Hafner, and D. Spišák, Understanding the complex metallic element Mn. I. Crystalline and noncollinear magnetic structure of α-Mn, Phys. Rev. B **68**, 014407 (2003).

[32] E. Fawcett, Spin-density-wave antiferromagnetism in chromium, Rev. Mod. Phys. **60**, 209 (1988).

[33] P. Dederichs, R. Zeller, H. Akai, and H. Ebert, Ab-initio calculations of the electronic structure of impurities and alloys of ferromagnetic transition metals, J. Magn. Magn. Mater. **100**, 241 (1991).

[34] A. Arrott and B. R. Coles, Antiferromagnetism of α − Mn and its alloys, J. Appl. Phys. **32**, S51 (1961).

[35] T. Yamada, N. Kunitomi, Y. Nakai, D. E. Cox, and G. Shirane, Magnetic structure of α − Mn, J. Phys. Soc. Jpn. **28**, 615 (1970).

[36] J. Marples, The lattice parameters of α-manganese at low temperatures, Phys. Lett. A **24**, 207 (1967).

[37] D. Legut and J. Pavlů, Electronic structure and elasticity of z-phases in the Cr–Nb–V–N system, J. Phys.: Condens. Matter **24**, 195502 (2012).

[38] M. E. Straumanis and C. C. Weng, The precise lattice constant and the expansion coefficient of chromium between +10 and +60° C, Acta Crystallogr. **8**, 367 (1955).

[39] W. Betteridge, The properties of metallic cobalt, Prog. Mater. Sci. **24**, 51 (1980).

[40] K. Hermann, Appendix e: Parameter tables of crystals, in *Crystallography and Surface Structure* (Wiley, 2011), pp. 265–266.

[41] R. P. Reed and R. E. Schramm, Lattice parameters of martensite and austenite in Fe-Ni alloys, J. Appl. Phys. **40**, 3453 (1969).

[42] M. Kadziolka-Gawel, W. Zarek, E. Popiel, and A. Chrobak, The crystal structure and magnetic properties of selected fcc FeNi and $Fe_{40}Ni_{40}B_{20}$ alloys, Acta Phys. Polonica A **117**, 412 (2010).

[43] M. E. Straumanis and C. L. Woodward, Lattice parameters and thermal expansion coefficients of Al, Ag and Mo at low temperatures. Comparison with dilatometric data, Acta Crystallogr. Sec. A **27**, 549 (1971).

[44] A. Wells, *Structural Inorganic Chemistry* (Oxford University Press, 1984).

[45] O. Schneeweiss, M. Friák, M. Dudová, D. Holec, M. Šob, D. Kriegner, V. Holý, P. Beran, E. P. George, J. Neugebauer, and A. Dlouhý, Magnetic properties of the CrMnFeCoNi high-entropy alloy, Phys. Rev. B **96**, 014437 (2017).

[46] M. Vaidya, K. Guruvidyathri, and B. Murty, Phase formation and thermal stability of CoCrFeNi and CoCrFeMnNi equiatomic high entropy alloys, J. Alloys Compd. **774**, 856 (2019).

[47] D. Ma, B. Grabowski, F. Körmann, J. Neugebauer, and D. Raabe, Ab initio thermodynamics of the CoCrFeMnNi high entropy alloy: Importance of entropy contributions beyond the configurational one, Acta Material. **100**, 90 (2015).

[48] W.-M. Choi, Y. H. Jo, S. S. Sohn, S. Lee, and B.-J. Lee, Understanding the physical metallurgy of the CoCrFeMnNi high-entropy alloy: An atomistic simulation study, npj Comp. Mater. **4**, 1 (2018).

[49] Z. Dong, S. Schönecker, W. Li, D. Chen, and L. Vitos, Thermal spin fluctuations in CoCrFeMnNi high entropy alloy, Sci. Rep. **8**, 12211 (2018).

[50] B. Cantor, Multicomponent and high entropy alloys, Entropy **16**, 4749 (2014).

[51] G. Laplanche, P. Gadaud, O. Horst, F. Otto, G. Eggeler, and E. George, Temperature dependencies of the elastic moduli and thermal expansion coefficient of an equiatomic, single-phase CoCrFeMnNi high-entropy alloy, J. Alloys Compd. **623**, 348 (2015).

[52] H. Cheng, Y.-C. Xie, Q.-H. Tang, C. Rao, and P.-Q. Dai, Microstructure and mechanical properties of FeCoCrNiMn high-entropy alloy produced by mechanical alloying and vacuum hot pressing sintering, Trans. Nonferrous Metals Soc. China **28**, 1360 (2018).

[53] Y. Ye, Y. Zhang, Q. He, Y. Zhuang, S. Wang, S. Shi, A. Hu, J. Fan, and Y. Yang, Atomic-scale distorted lattice in chemically disordered equimolar complex alloys, Acta Material. **150**, 182 (2018).

[54] S. Wang, Atomic structure modeling of multi-principal-element alloys by the principle of maximum entropy, Entropy **15**, 5536 (2013).

[55] Z. Wu, M. Troparevsky, Y. Gao, J. Morris, G. Stocks, and H. Bei, Phase stability, physical properties and strengthening mechanisms of concentrated solid solution alloys, Curr. Opin. Solid State Mater. Sci. **21**, 267 (2017).

[56] H. Ge, H. Song, J. Shen, and F. Tian, Effect of alloying on the thermal-elastic properties of 3d high-entropy alloys, Mater. Chem. Phys. **210**, 320 (2018).

[57] C. Niu, C. R. LaRosa, J. Miao, M. J. Mills, and M. Ghazisaeidi, Magnetically-driven phase transformation strengthening in high entropy alloys, Nat. Commun. **9**, 1363 (2018).

[58] C. Niu, A. J. Zaddach, A. A. Oni, X. Sang, J. W. Hurt, J. M. LeBeau, C. C. Koch, and D. L. Irving, Spin-driven ordering of Cr in the equiatomic high entropy alloy NiFeCrCo, Appl. Phys. Lett. **106**, 161906 (2015).

[59] M. Gutierrez, G. Rodriguez, G. Bozzolo, and H. Mosca, Melting temperature of CoCrFeNiMn high-entropy alloys, Comput. Mater. Sci. **148**, 69 (2018).

[60] W. Ji, W. Wang, H. Wang, J. Zhang, Y. Wang, F. Zhang, and Z. Fu, Alloying behavior and novel properties of CoCrFeNiMn high-entropy alloy fabricated by mechanical alloying and spark plasma sintering, Intermetallics **56**, 24 (2015).

[61] F. Otto, Y. Yang, H. Bei, and E. George, Relative effects of enthalpy and entropy on the phase stability of equiatomic high-entropy alloys, Acta Material. **61**, 2628 (2013).

[62] See Supplemental Material at http://link.aps.org/supplemental/10.1103/PhysRevMaterials.3.124410 for DOS of molybdenum based derivatives.